AJNR

Automated quantification of cerebral microbleeds in susceptibility-weighted MRI: association with vascular risk factors, white matter hyperintensity burden, and cognitive function

Ji Su Ko, Yangsean Choi, Eun Seon Jeong, Hyun-Jung Kim, Grace Yoojin Lee, Ji Eun Park, Namkug Kim and Ho Sung Kim

AJNR Am J Neuroradiol published online 23 October 2024
http://www.ajnr.org/content/early/2024/10/23/ajnr.A8552

Published October 23, 2024 as 10.3174/ajnr.A8552

ORIGINAL RESEARCH

Automated quantification of cerebral microbleeds in susceptibility-weighted MRI: association with vascular risk factors, white matter hyperintensity burden, and cognitive function

Ji Su Ko, Yangsean Choi, Eun Seon Jeong, Hyun-Jung Kim, Grace Yoojin Lee, Ji Eun Park, Namkug Kim, Ho Sung Kim

ABSTRACT

BACKGROUND AND PURPOSE: To train and validate a deep learning (DL)-based segmentation model for cerebral microbleeds (CMB) on susceptibility-weighted MRI; and to find associations between CMB, cognitive impairment, and vascular risk factors.

MATERIALS AND METHODS: Participants in this single-institution retrospective study underwent brain MRI to evaluate cognitive impairment between January–September 2023. For training the DL model, the nnU-Net framework was used without modifications. The DL model's performance was evaluated on independent internal and external validation datasets. Linear regression analysis was used to find associations between log-transformed CMB numbers, cognitive function (mini-mental status examination [MMSE]), white matter hyperintensity (WMH) burden, and clinical vascular risk factors (age, sex, hypertension, diabetes, lipid profiles, and body mass index).

RESULTS: Training of the DL model (n = 287) resulted in a robust segmentation performance with an average dice score of 0.73 (95% CI, 0.67–0.79) in an internal validation set, (n = 67) and modest performance in an external validation set (dice score = 0.46, 95% CI, 0.33–0.59, n = 68). In a temporally independent clinical dataset (n = 448), older age, hypertension, and WMH burden were significantly associated with CMB numbers in all distributions (total, lobar, deep, and cerebellar; all *P* <.01). MMSE was significantly associated with hyperlipidemia (β = 1.88, 95% CI, 0.96–2.81, *P* <.001), WMH burden (β = -0.17 per 1% WMH burden, 95% CI, -0.27-0.08, P <.001), and total CMB number (β = -0.01 per 1 CMB, 95% CI, -0.02-0.001, *P* = .04) after adjusting for age and sex.

CONCLUSIONS: The DL model showed a robust segmentation performance for CMB. In all distributions, CMB had significant positive associations with WMH burden. Increased WMH burden and CMB numbers were associated with decreased cognitive function.

ABBREVIATIONS: CMB = cerebral microbleed; DL = deep learning, DSC = dice similarity coefficient; MMSE = mini-mental status examination; SVD = small vessel disease; SWI = susceptibility-weighted image; WMH = white matter hyperintensity.

Received month day, year; accepted after revision month day, year.
Department of Radiology and Research Institute of Radiology, (J.S.K., Y.C., E.S.J., J.E.P., H.S.K.) University of Ulsan College of Medicine, Asan Medical Centre, Seoul, Republic of Korea, and Department of Convergence Medicine (H.J.K., G.Y.L., N.K.), University of Ulsan College of Medicine, Asan Medical Centre, Seoul, Republic of Korea.

The authors declare no conflicts of interest related to the content of this article

Please address correspondence to Yangsean Choi, MD, PhD, Department of Radiology and Research Institute of Radiology, University of Ulsan College of Medicine, Asan Medical Centre, 88, Olympic-ro 43-gil, Songpa-gu, Seoul, 05505, Republic of Korea; email: phillipchoi007@gmail.com.

SUMMARY SECTION

PREVIOUS LITERATURE: Previous studies have focused on the DL model's segmentation performance of CMB, but no studies have investigated the association between automated CMB segmentations and clinical variables.

KEY FINDINGS: The DL model demonstrated robust segmentation performance with an average DSC of 0.73 in the internal validation set. WMH burden had a significant association with CMB number in all distributions. MMSE had a significant negative association with WMH burden and total CMB number after adjusting for age and sex.

KNOWLEDGE ADVANCEMENT: These findings highlight the potential of automated CMB segmentation, using DL models, to further understand its clinical implications in the future.

INTRODUCTION

Cerebral microbleeds (CMB) are small areas of microhemorrhages visible as dark signal intensity on susceptibility-weighted images (SWI) or T2* gradient echo sequences of brain MRI. Typically ranging 5–10 mm, they are regarded as silent indicators preceding potential future intracranial hemorrhages.[1] CMB is characterized by localized clusters of macrophages containing paramagnetic hemosiderin,[2] which leads to signal attenuation on SWI or T2* gradient echo sequences owing to susceptibility effects. SWI is the preferred sequence for detecting CMB (over T2* gradient echo sequences) due to its higher detection rate.[3] It has become increasingly available for brain MRI, leading to increased incidental detection of CMB, with a true-positive detection rate of 48–89%.[1]

CMB is a common imaging finding in patients with small vessel diseases (SVD), with up to 36% of adults aged 80 to 90 demonstrating evidence of CMB.[4] Since CMB is an imaging marker of SVD, we hypothesized that the degree of CMB may be associated with an established vascular risk factor such as obesity, hypertension, diabetes, and hyperlipidemia.[1,5–8] These risk factors are also associated with the development of Alzheimer's dementia,[9] and CMB may, therefore, be associated with both. A previous study demonstrated that cognitive impairment reflected in low mini-mental status examination (MMSE) scores is associated with an increased number of CMBs.[10] Moreover, cerebral white matter hyperintensity (WMH)—a common imaging finding in the elderly—has a significant positive association with CMB.[5]

To examine the relationship between CMB and clinical factors, accurate quantification of CMB is needed. In many previous studies, CMB was quantified through visual assessment.[1,5,6,10,11] However, common imaging findings that mimic CMB included, dilated cortical veins, iron accumulation in the basal ganglia, and calcifications.[12] Previous studies have reported a wide range of interrater reliability for CMB quantification with kappa values of 0.33–0.88.[13] Moreover, manual counting of CMB is laborious and may be superseded by automated deep learning (DL)-based CMB quantification.

The recent advancement of DL-based models has shown great promise in various medical image segmentation challenges.[14] Particularly, no-new-Net (nnU-Net), a self-configuring DL-based framework, has been found to outperform most other DL-based models in various segmentation tasks.[15] Unlike the excellent segmentation performances in glioblastoma [16] or intracranial hemorrhage,[17] relatively few segmentation tasks have been studied in CMB.[12,18]

However, the simultaneous automated quantification of CMB and validation of their clinical significance is not well established in the literature. Therefore, this study aimed to evaluate the performance of a DL-based segmentation model in quantifying CMB on SWI, and to investigate the relationship between CMB amount, various vascular risk factors, WMH burden, and cognitive function in participants suspected to be in cognitive decline.

MATERIALS AND METHODS

The institutional review board of Asan Medical Center approved this single-center retrospective cohort study with a waiver of informed consent forms (IRB No. S2023-1027-0001). This study adhered to the methodology proposed in the CLAIM checklist (**Table S1**).

Study participants

The participants were patients who had been clinically suspected to be cognitively impaired, and who had undergone a brain MRI between January – August 2023 at our tertiary referral hospital. The brain MRIs of these participants were used for training and validating a DL-based segmentation model. Those with CMB were randomly divided into a 7:3 ratio, with 30% of the participants allocated to the internal validation dataset and the remaining 70%, along with the CMB absent group, allocated to the training dataset. Participants assessed between April–August 2023 were included for clinical analysis. The inclusion criteria were: age > 18 years, and an available brain MRI with SWI and filtered phase images. Baseline clinical information, including diabetes, hypertension, hyperlipidemia, lipid profiles (total cholesterol, triglyceride, and high- and low-density lipoproteins), and body-mass index, was retrieved from the electronic medical records, and MMSE based cognitive scores were collected. The MMSE had multiple components, including temporo-spatial orientation, memory registration, attention and calculation, memory recall, language, and space-time configuration. The maximum score was 30. Participants were excluded if any of the clinical information (*i.e.* diabetes, hypertension, total cholesterol level, MMSE scores) was missing within one year of the MRI scan (**Figure 1**).
Moreover, an independent external validation dataset was collected for the DL segmentation model performance evaluation. The eligibility criteria for the external validation dataset were: adult participants who had undergone a brain MRI with available SWI and filtered phase images from outside hospitals during January–December 2023, who had visited our tertiary referral hospital. The selection process for eligible participants is depicted in **Figure 1**.

MR acquisition parameters

All MRIs were acquired using a 3.0-T scanner (Ingenia CX, Philips Healthcare) using a 32-channel head coil. The dedicated brain MRI protocol included three-dimensional 1-mm isovoxel T1-weighted sequence (repetition time/echo time/inversion time [m/s], 6.3/2.9/0), two-dimensional axial FLAIR images (9000/95/2500), T2-weighted images (3000/80/0), and SWI/filtered phase images, which were postprocessed from multi-echo gradient images (31/19.6; four echoes, with echo spacing of 6.2 m/s) according to the scanner's standard settings (**Table S2**).

MRI preprocessing and manual CMB segmentation labeling

Initially, SWI and the filtered phase images were stored as DICOM formats, which were converted into NIfTI file formats.[19] The images then underwent DL-based automated brain extraction using HD-BET.[20] Subsequently, all images underwent N4 bias field correction for intensity normalization.[21] For ground truth segmentation masks, all visible CMB on SWI and phase images were manually segmented by a neuroradiologist (J.S.K. with 5 years of experience in diagnostic neuroradiology) using a 3D Slicer (version 5.6.1). A supervising neuroradiologist then reviewed the segmentations and made modifications where necessary (Y.C. with 10 years of experience in diagnostic neuroradiology). Finally, a pretrained DL-based model was used for whole-brain segmentation (SynthSeg).[22] Briefly, SynthSeg is a whole-brain segmentation tool that is robust against a wide range of contrasts and resolutions, thus providing SWI-based reliable anatomical maps. Since SynthSeg outputs were generated from native SWI images, co-registration or transformation of the images was not executed. The segmentation outputs included cerebral white matter, the hippocampus, amygdala, cerebellum, brainstem, thalamus, caudate, putamen, pallidum, and nucleus accumbens.

Training and inference of the DL segmentation model

The DL segmentation model was solely trained on the basis of nnU-Net without any modification.[15] The nnU-Net architecture provides self-configured pre-processing steps, including automatic cropping of the image peripheries, resampling to resolutions equal to the ground truth segmentation masks, and z-transform normalization. The two-channel three-dimensional input images were SWI and filtered-phase images. For each training, the dataset was randomly divided into five folds for cross-validation, with each fold completing 1000 epochs of training. The best-performing model with the highest average dice similarity coefficient (DSC) values in the validation set was chosen.

The CMB outputs were co-registered with corresponding SynthSeg-generated brain MRI outputs. The CMB were then categorized based on their location: 1) lobar: cerebral white matter and cortex; 2) deep (brainstem, thalamus, caudate, putamen, pallidum, and nucleus accumbens); and 3) cerebellar. **Figure 2** shows the summarized workflow for image preprocessing and training a DL segmentation model. The codes used for preprocessing and model inference are provided on a GitHub page (https://github.com/olnsnlyy/CMB_segment).

Automated WMH burden quantification

WMH, visible on two-dimensional axial FLAIR images, was automatically quantified via commercial software (LesionQuant module of the NeuroQuant, CorTechs Labs, San Diego, CA, USA). The two-dimensional FLAIR images of all participants were spatially aligned and reconstructed based on three-dimensional T1-weighted images. The WMH burden was calculated as WMH volumes divided by the total intracranial volumes. Both radiologists reviewed all WMH segmentations without making any further modifications.

Statistical analysis

Continuous variables between participants according to CMB presence were compared using a two-sided independent *t*-test. Categorical variables were compared using Pearson's chi-squared test. DSC was used to evaluate the performance of the CMB segmentation model in independent internal and external validation datasets. DSC measures the volumetric overlap between the predicted and ground truth CMB contours.[23] Moreover, the sensitivity, specificity, and accuracy of CMB prediction in an external validation dataset were calculated and compared with the ground truth by the radiologist. Linear regression analysis was performed to find associations between clinical variables and log-transformed CMB numbers. Post-hoc subgroup linear regression analyses were performed to find associations between log-transformed CMB numbers by their distribution (*i.e.,* deep, lobar, and cerebellar) and clinical variables. Additionally, linear regression investigated the association between clinical variables, WMH burden, log-transformed CMB numbers by their distribution, and MMSE scores. A multivariable linear regression analysis including age, sex, diabetes, hyperlipidemia, total cholesterol, WMH burden, and total CMB number was performed with the MMSE score as the dependent variable. Furthermore, participants were stratified based on CMB numbers (none, 1–10, and >10) and their location. MMSE scores were then compared using the Kruskal-Wallis test with post-hoc comparisons. Finally, additional linear regression analyses were performed to examine the association between MMSE scores and CMB numbers (none, 1–10, and >10), separately for each CMB distribution (total, lobar, deep, and cerebellar). The adjusted coefficient of determination (R^2) was calculated for each model. Statistical significance was set at a *P*-value of <.05. R statistical software (version 4.2.1; R Foundation for Statistical Computing) was used for all statistical analyses.

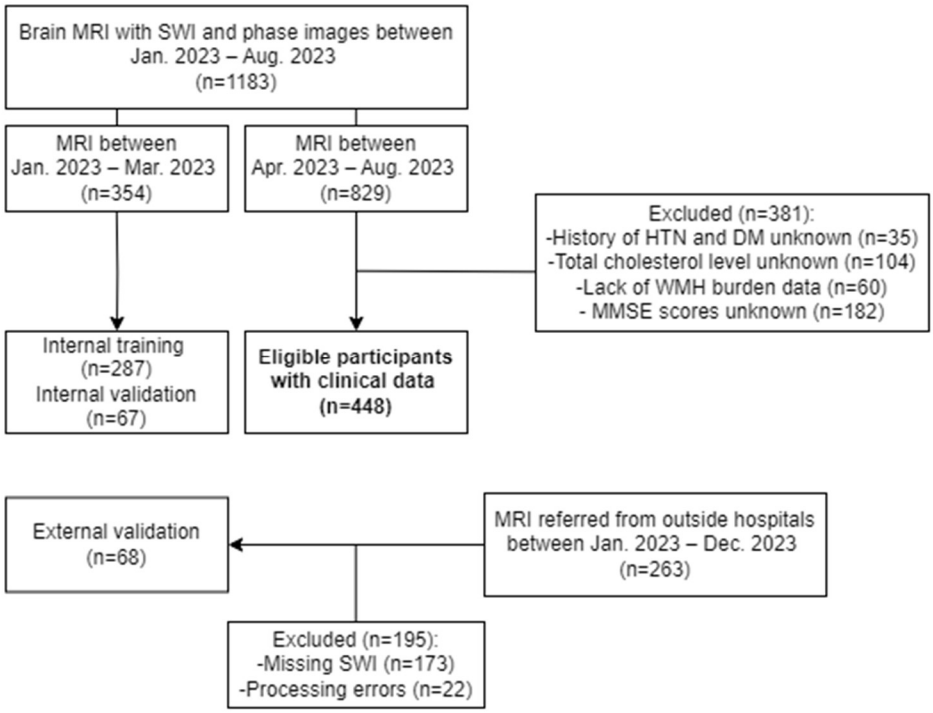

FIG 1. A flowchart for selecting eligible study participants.

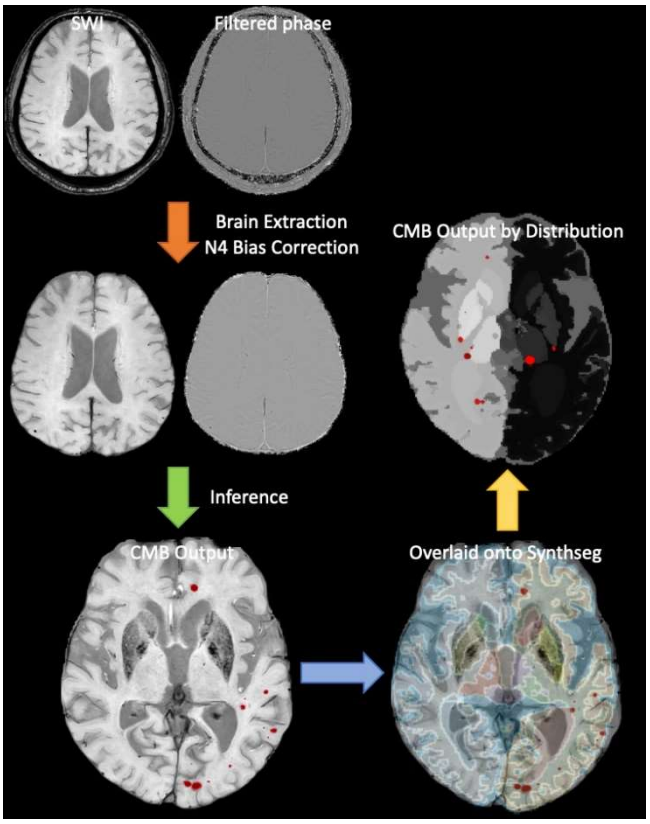

Fig 2. Schematic workflow of image preprocessing and CMB segmentation output inference.

RESULTS

Baseline characteristics of the study participants

Table 1 summarizes the baseline characteristics of all participants. Among 1,183 consecutive participants with suspected cognitive decline, 354 were included for the training dataset (n = 287; mean age, 68 ± 14; 116 [40.4%] male and 171 [59.6%] female) and internal validation dataset (n = 67; mean age, 72 ± 10; 27 [40.3%] male and 40[59.7%] female) for a DL segmentation model. Among 829 participants with clinical information, 381 were excluded for missing information on either hypertension or diabetes (n = 35), total cholesterol levels (n = 104), WMH burden data (n = 60), and MMSE (n = 182), leaving 448 eligible participants (mean age, 72 ± 9 years; 171 [38.2%] male and 277 [61.8%] female).

Between January–December 2023, 263 brain MRI studies were referred to our center, of which 195 were excluded for missing SWI (n = 173) and segmentation processing errors (n = 22). Sixty-eight participants from 49 different sites were involved (mean age, 52 ± 17 years; 32 [47%] male and 36 [53] female). Seventeen unique MR scanner models (four 1.5T and 13 3T) were included from three major manufacturers (GE HealthCare, Philips Healthcare, and Siemens Healthineers). The slice thicknesses ranged between 0.8–5 mm, and the in-plane spatial resolutions ranged between 0.24 × 0.24 – 0.9 × 0.9 mm^2 (**Table S3**).

CMB segmentation evaluation

The internal and external validation datasets mean DSCs were 0.73 ± 0.25 (95% CI, 0.67–0.79) and 0.46 ± 0.32 (95% CI, 0.33–0.59), respectively. In the internal validation dataset, the DL segmentation model demonstrated a F1 score and sensitivity of 61.8% (43.8–79.8%) and 85.7% (70.6–93.7%), respectively. In the external validation dataset, the DL segmentation model performed modestly with an accuracy, sensitivity, and specificity of 75.0 (63.6–83.8%), 70.0 (48.1–85.5%), and 77.1% (63.5–86.7%), respectively (**Table S3**). Representative images of CMB segmentations are illustrated in **Figure 3**. Moreover, example images of false positive and false negative segmentations in the external validation dataset are provided in **Supplementary Figure 1**.

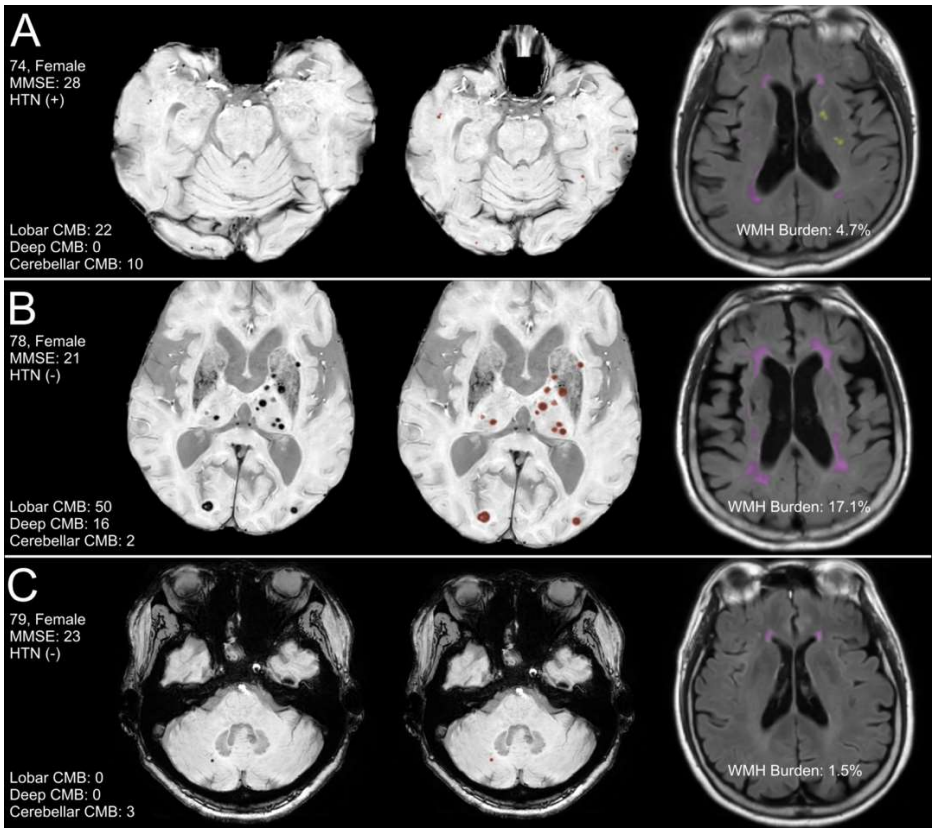

Fig 3. Representative images of SWI, CMB (red) and WMH (purple; periventricular white matter, yellow; deep white matter) segmentations overlaid on SWI and FLAIR in three participants. (a) 74-year-old female with normal cognition and mild WMH

burden, with lobar and cerebellar CMB; (b) 78-year-old female with impaired cognition and large WMH burden, with increased CMB numbers in all three locations; and (c) 79-year-old female with impaired cognition and minimal WMH burden, with only a few cerebellar CMB.

Comparison between participants according to CMB

Participants with CMB were significantly older than those without CMB (73 ± 9 vs. 69 ± 10, respectively; P <.001). The difference in MMSE between the two groups was marginally significant (CMB present, 23.8 ± 5.5; CMB absent, 24.8 ± 4.8; P = .053). Participants with CMB had a significantly higher WMH burden (4.8 ± 5.6%) than those without CMB (2.4 ± 3.2%) (P <.001). All other clinical variables were not significantly different between the two groups (CMB present vs. absent) (**Table 2**).

Relationship between the CMB number and clinical variables

In the training dataset, no significant differences were observed between the ground truth-based and inference-based CMB counts, with both showing a negative association with total cholesterol, HDL, LDL, and a positive association with WMH burden. In the clinical dataset, WMH burden had significant positive associations with log-transformed CMB in all areas (total, β = 0.08, 95% CI = 0.06–0.1, P <.001; lobar, β = 0.07, 95% CI = 0.05–0.09, P <.001; deep, β = 0.04, 95% CI = 0.03–0.05, P <.001; cerebellar, β = 0.02, 95% CI = 0.01–0.03, P <.001) (**Figure 4, Online Supplemental Data**). Older age and hypertension were also significantly associated with log-transfomed CMB in all areas. Total cholesterol level revealed a negative association with log-transformed total, lobar, and deep CMB number (total CMB, β = -0.003, 95% CI = -0.006–0.001, P = .007; lobar CMB, β = -0.003, 95% CI = -0.005–0.001, P = .005; deep CMB, β = -0.002, 95% CI = -0.003–0.001, P = .002). HDL and LDL levels showed a negative association with log-transformed CMB in all areas, with statistically significant associations observed between HDL and deep CMB (β = -0.003, 95% CI = -0.007–0.002, P = .04, and LDL and lobar CMB (β = -0.003, 95% CI = -0.006–0.005, P = .02) (**Online Supplemental Data**).

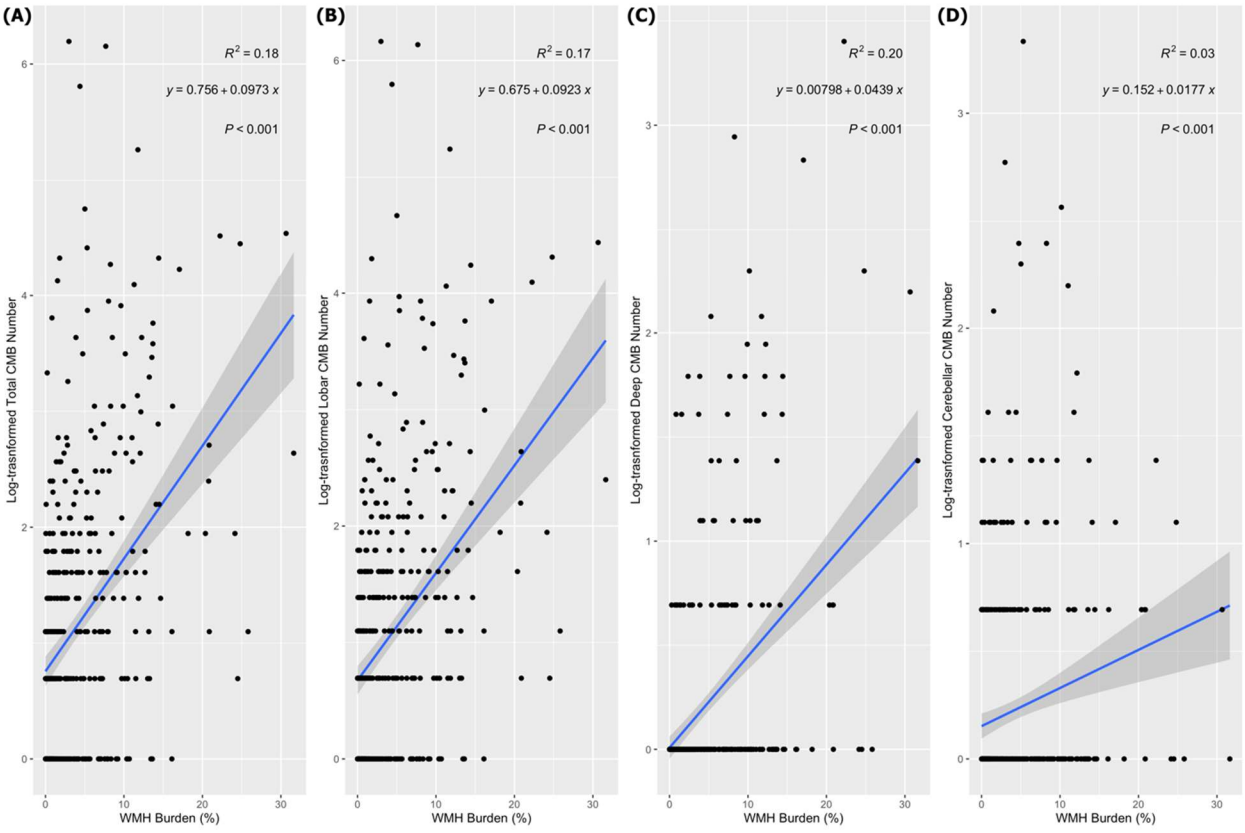

Fig 4. Relationship between CMB number and WMH burden. These scatterplots illustrate associations between the log-transformed CMB number by their distribution and WMH burden. Among these, lobar CMB numbers show the highest beta coefficient with WMH burden (β = 0.09, P <.001). Solid blue lines indicate the lines of best fit of linear regression and the shaded

areas indicate the 95% confidence intervals. The R^2 values are coefficients of determination of linear regression.

Relationship between the MMSE and clinical variables

In univariable linear regression, age; diabetes; hyperlipidemia; total cholesterol; WMH burden; and total CMB numbers demonstrated significant associations with MMSE scores (age, β = -0.19, 95% CI = -0.24–-0.14, *P* <.001; diabetes, β = -1.15, 95% CI = -2.26–-0.04, *P* = .043; hyperlipidemia, β = 1.51, 95% CI = 0.52–2.51, *P* = .003; total cholesterol, β = 0.02, 95% CI = 0.003–0.03, *P* = .014; WMH burden, β = -0.29, 95% CI = -0.38–-0.19, *P* <.001; total CMB number, β = -0.014, 95% CI = -0.03–-0.006, *P* = .006). Univariable linear regression analyses between log-transformed CMB numbers in each area and MMSE scores showed that total, deep, and lobar CMB numbers had strong negative associations with MMSE (total, β = -0.66, *P* = .001; deep, β = -1.2, *P* = .033; lobar, β = -0.61, *P* = .004) (**Supplementary Figure 2**). In multivariable linear regression, all variables except for total cholesterol and diabetes showed significant associations with MMSE scores (**Table 3**). Additionally, the group with >10 lobar CMB had significantly lower MMSE scores than those with fewer lobar CMB (*P* = .03) and no lobar CMB (*P* = .021) (**Figure 5**).

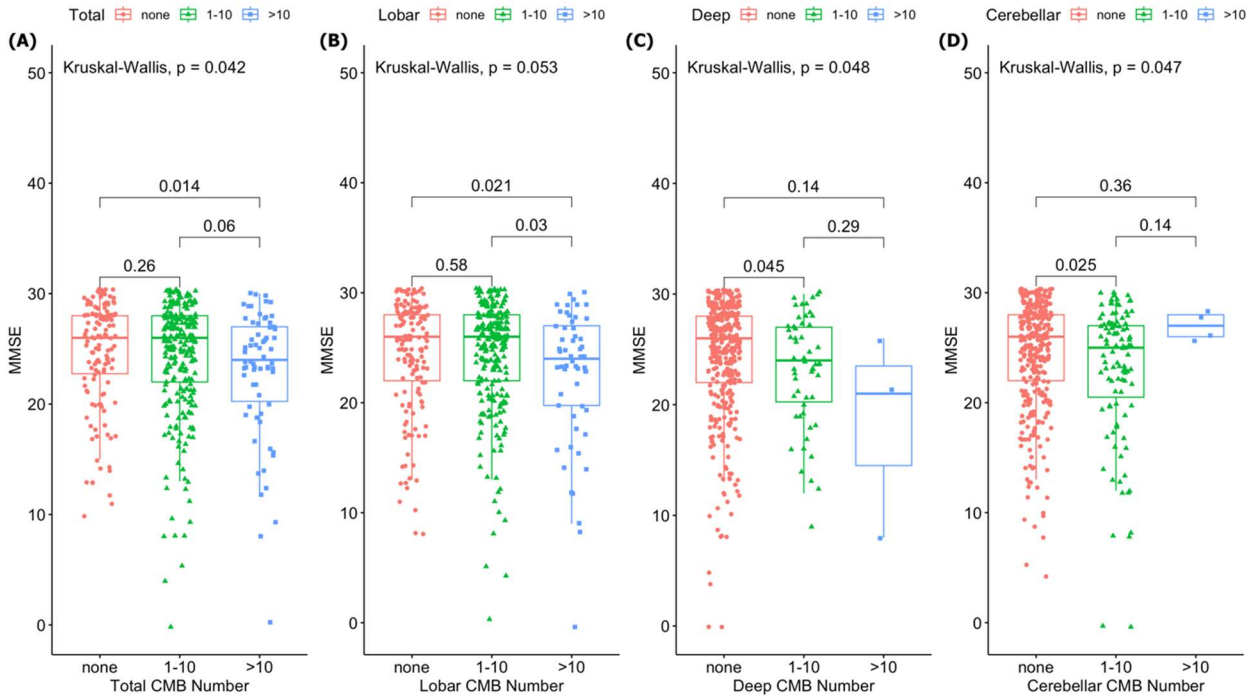

Fig 5. Boxplots showing the group-comparisons of MMSE scores with respect to CMB numbers (none, 1–10, and >10). Significant group differences in MMSE scores are observed among the three groups of CMB numbers (total [A], deep [C], and cerebellar [D]). The group with >10 lobar CMB (B) has significantly lower MMSE scores than those with fewer lobar CMB (P = .03) and no lobar CMB (P = .021).

DISCUSSION

Our aims were to train and validate a DL segmentation model for accurate CMB quantification, and to evaluate associations among CMB numbers, WMH burden, vascular risk factors, and cognitive function. The segmentation performance was robust in the internal validation dataset (DSC = 0.73) but only modest in the external validation dataset (DSC = 0.46). In all locations, CMB numbers had significant positive associations with WMH burden, older age, and hypertension. Particularly, lobar and deep CMB numbers were significantly associated with lower total cholesterol levels. In multivariable linear regression analysis, older age, male gender, hyperlipidemia, a higher total CMB number, and WMH burden were associated with decreased cognitive function.
In the internal validation dataset, the robust segmentation performance was similar to the results observed in a previous study

investigating DL-based CMB segmentation (DSC = 0.72).[24] Nonetheless, the DSC of the external validation dataset was noticeably lower than that of the internal validation dataset. This discrepancy is probably attributable to the highly variable MR acquisition settings within the external validation dataset, differing in MR manufacturers, magnetic fields, in-plane resolutions, and slice thicknesses. Moreover, the mean age of the external dataset was significantly lower than that of internal dataset, which may also have affected the segmentation performance. Despite the lower DSC in the external validation dataset, the DL model's CMB detection rate was acceptable, which is promising considering that true positive CMB detection is clinically more relevant than accurate volumetric segmentation. More importantly, the DL model's generalizability has been proven by the robust external validation dataset.

In recent years, several automated approaches for CMB detection have been proposed. One notable method utilized a two-stage framework based on a 3D fast radial symmetry transform and deep residual neural networks, achieving a sensitivity of 95.8% with a precision of 70.9%, and 1.6 false positives per case.[12] However, this study lacked external validation and used a relatively small dataset. Another approach employed a regional-based You Only Look Once (YOLO) for candidate detection followed by a 3D-CNN for false positive reduction, demonstrating a sensitivity of 93.62% and 78.85% for high and low-resolution data, respectively.[25] Despite its efficacy, the complex DL structure of these two studies have been limited in their adaptability compared to simpler models like nnU-net, which our study utilizes. Lastly, a study focusing on traumatic brain injury cases compared classification and segmentation approaches, finding the U-Net model to be the most effective with a 90% detection rate at false positive counts of 17.1 in patients with traumatic brain injury.[18] However, its limited scope in relation to traumatic brain injury cases and the small dataset size raises questions about the generalizability of the results. Our approach, utilizing the nnU-net model, offers a simpler yet efficient alternative, providing a modest performance while maintaining a straightforward architecture that facilitates potential modifications and adaptability.

Older age and hypertension are well-established risk factors for CMB.[1] However, an interesting finding was that the total, deep, and lobar CMB number was negatively associated with total cholesterol levels. Several studies have also found a negative association between lipid profiles and CMB prevalence.[6,7,26] A large cross-sectional study of neurologically healthy individuals in Japan revealed an inverse correlation between total cholesterol levels and the prevalence of deep CMB.[7] In other studies, the serum low-density lipoprotein level was negatively correlated with deep CMB,[6] while the Framingham heart study showed a negative association between total cholesterol and lobar CMB.[26] Reduced levels of total cholesterol have been associated with smooth muscle deterioration and endothelial cells weakness, making arterial walls more fragile and prone to microaneurysm development, potentially causing leakage and rupture.[8]

CMB and WMH are the most common radiologic manifestations of SVD; they frequently coexist in patients with SVD and share an identical pathological basis.[27,28] However, visual assessments of WMH, such as the Fazekas scale, have limited value for the accurate volumetric quantification of WMH. Balestrieri *et al.*[5] measured WMH volume using a semi-automated method, finding a significant positive correlation between CMB and WMH volume. Herein, the lobar CMB number exhibited the highest positive association with WMH burden, suggesting a potential link between lobar CMB and WMH stemming from cerebral amyloid angiopathy.[29–31]

Several studies have investigated the association between cognitive function and SVD imaging findings, including CMB and WMH. Zamboni *et al.* demonstrated that in patients with transient ischemic attacks, reduced cognitive function was linked to an increased probability of WMH in the frontal periventricular white matter.[32] Poels *et al.* discovered that the links between deep or cerebellar CMB and cognitive function were weaker compared to strictly lobar CMB and influenced by other factors such as brain atrophy and SVD indicators . In contrast, the association between lobar CMB and cognition was found to be highly significant.[10] Likewise, the lobar CMB number exhibited the strongest negative association with cognition among the CMB distribution patterns, suggesting that strictly lobar CMB may indicate pathologies related to cerebral amyloid angiopathy, such as the vascular accumulation of beta-amyloid, which may directly affect cognition.[10,33] Another hypothesis suggests that strictly lobar CMBs may have a more pronounced impact on surrounding brain tissue compared to deep or cerebellar CMBs due to their potential to disrupt functionally significant cortical and subcortical structures.[34] Moreover, the MMSE scores were lower in the CMB-lobar group compared to the CMB-mixed group, indicating that lobar CMB related to cerebral amyloid angiopathy may contribute significantly to the pathological process of cognitive decline.[35]

This study has a few limitations. First, there is the inherent bias associated with the retrospective nature of this study. Second, a few participants were excluded due to missing information on body mass index and detailed lipid profiles (*i.e.*, triglyceride and high- and low-density lipoproteins). Third, only the MMSE was used to assess cognitive function. This may have limited our comprehension of the impact of CMB in various cognitive domains. Fourth, the DL segmentation model was trained in a single center; subsequently, the segmentation performance in the external validation dataset was only modest. However, such underperformance was anticipated since DL models trained with medical images have consistently shown lower performances in external validation datasets.[36] Further research is needed to improve the technical aspects of the DL segmentation model for CMB. Fifth, when comparing the demographics among the training dataset, internal validation dataset, and clinical dataset, a significant

difference was observed in age, suggesting that there might be discrepancies between the groups. However, no significant differences were found in other clinical variables or the CMB count. Sixth, we did not exclude patients with medication histories that may have acted as confounding factors. However, since each dataset involves a relatively similar cohort group that visited the hospital for mild cognitive impairment or dementia, the impact is expected to be minimal. Finally, reports suggest that vessel wall thickening, enlarged perivascular space, decreased vascular density, cerebral blood flow, and increased vessel tortuosity are associated with SVD. However, in our study, we did not analyze the association between these factors and CMBs.[37,38] Finally, our study population only included participants suspected of clinical impairment and our results cannot, therefore, be generalized.

CONCLUSIONS

The DL segmentation model accurately quantified CMB in all locations. After adjusting for age and sex, multivariable linear regression revealed that hyperlipidemia, a higher total cerebral microbleed number, and WMH burden were associated with decreased cognitive function. Our study efficiently analyzed CMB and WMH burdens and explored their clinical relevance regarding cognitive function.

ACKNOWLEDGMENTS

This study was supported by a grant (2024IP0026) from the Asan Institute for Life Sciences, Asan Medical Center, Seoul, Korea.

REFERENCES

1. 1. Haller S, Vernooij MW, Kuijer JPA, et al. Cerebral Microbleeds: Imaging and Clinical Significance. Radiology 2018;287:11–28.
2. 2. Fazekas F, Kleinert R, Roob G, et al. Histopathologic analysis of foci of signal loss on gradient-echo T2*-weighted MR images in patients with spontaneous intracerebral hemorrhage: evidence of microangiopathy-related microbleeds. AJNR Am J Neuroradiol 1999;20:637–42.
3. 3. Shams S, Martola J, Cavallin L, et al. SWI or T2*: Which MRI Sequence to Use in the Detection of Cerebral Microbleeds? The Karolinska Imaging Dementia Study. American Journal of Neuroradiology 2015;36:1089–95.
4. 4. Sharrief A. Diagnosis and Management of Cerebral Small Vessel Disease. CONTINUUM: Lifelong Learning in Neurology 2023;29:501–18.
5. 5. Balestrieri A, Lucatelli P, Suri HS, et al. Volume of White Matter Hyperintensities, and Cerebral Micro-Bleeds. Journal of Stroke and Cerebrovascular Diseases 2021;30:105905.
6. 6. Zhao Y, Zhou Y, Zhou H, et al. Low-density lipoprotein cholesterol, statin therapy, and cerebral microbleeds: The CIRCLE study. Neuroimage Clin 2023;39:103502.
7. 7. Mitaki S, Nagai A, Oguro H, et al. Serum Lipid Fractions and Cerebral Microbleeds in a Healthy Japanese Population. Cerebrovasc Dis 2017;43:186–91.
8. 8. Konishi M, Iso H, Komachi Y, et al. Associations of serum total cholesterol, different types of stroke, and stenosis distribution of cerebral arteries. The Akita Pathology Study. Stroke 1993;24:954–64.
9. 9. Gottesman RF, Schneider ALC, Zhou Y, et al. Association Between Midlife Vascular Risk Factors and Estimated Brain Amyloid Deposition. JAMA 2017;317:1443.
10. 10. Poels MMF, Ikram MA, van der Lugt A, et al. Cerebral microbleeds are associated with worse cognitive function: the Rotterdam Scan Study. Neurology 2012;78:326–33.
11. 11. Poels MMF, Vernooij MW, Ikram MA, et al. Prevalence and risk factors of cerebral microbleeds: an update of the Rotterdam scan study. Stroke 2010;41:S103-106.
12. 12. Liu S, Utriainen D, Chai C, et al. Cerebral microbleed detection using Susceptibility Weighted Imaging and deep learning. NeuroImage 2019;198:271–82.
13. 13. Cordonnier C, Potter GM, Jackson CA, et al. Improving Interrater Agreement About Brain Microbleeds. Stroke 2009;40:94–9.
14. 14. Wang R, Lei T, Cui R, et al. Medical image segmentation using deep learning: A survey. IET Image Processing 2022;16:1243–67.
15. 15. Isensee F, Jaeger PF, Kohl SAA, et al. nnU-Net: a self-configuring method for deep learning-based biomedical image segmentation. Nat Methods 2021;18:203–11.
16. 16. Eijgelaar RS, Visser M, Müller DMJ, et al. Robust Deep Learning–based Segmentation of Glioblastoma on Routine Clinical MRI Scans Using Sparsified Training. Radiology: Artificial Intelligence 2020;2:e190103.
17. 17. Mansour RF, Aljehane NO. An optimal segmentation with deep learning based inception network model for intracranial hemorrhage

diagnosis. Neural Comput & Applic 2021;33:13831–43.
18. 18. Koschmieder K, Paul MM, van den Heuvel TLA, et al. Automated detection of cerebral microbleeds via segmentation in susceptibility-weighted images of patients with traumatic brain injury. NeuroImage: Clinical 2022;35:103027.
19. 19. Li X, Morgan PS, Ashburner J, et al. The first step for neuroimaging data analysis: DICOM to NIfTI conversion. Journal of Neuroscience Methods 2016;264:47–56.
20. 20. Isensee F, Schell M, Pflueger I, et al. Automated brain extraction of multisequence MRI using artificial neural networks. Hum Brain Mapp 2019;40:4952–64.
21. 21. Tustison NJ, Avants BB, Cook PA, et al. N4ITK: Improved N3 Bias Correction. IEEE Transactions on Medical Imaging 2010;29:1310–20.
22. 22. Billot B, Greve DN, Puonti O, et al. SynthSeg: Segmentation of brain MRI scans of any contrast and resolution without retraining. Medical Image Analysis 2023;86:102789.
23. 23. Thada V. Comparison of Jaccard, Dice, Cosine Similarity Coefficient To Find Best Fitness Value for Web Retrieved Documents Using Genetic Algorithm. International Journal of Innovations in Engineering and Technology 2013;2.
24. 24. Fan P, Shan W, Yang H, et al. Cerebral Microbleed Automatic Detection System Based on the "Deep Learning." Front Med 2022;9.
25. 25. Al-Masni MA, Kim W-R, Kim EY, et al. Automated detection of cerebral microbleeds in MR images: A two-stage deep learning approach. Neuroimage Clin 2020;28:102464.
26. 26. Romero JR, Preis SR, Beiser A, et al. Risk factors, stroke prevention treatments, and prevalence of cerebral microbleeds in the Framingham Heart Study. Stroke 2014;45:1492–4.
27. 27. Gao Z, Wang W, Wang Z, et al. Cerebral Microbleeds Are Associated with Deep White Matter Hyperintensities, but Only in Hypertensive Patients. PLoS One 2014;9:e91637.
28. 28. Zhao X, Yin L, Yu L, et al. Correlation study and clinical value analysis between cerebral microbleeds and white matter hyperintensity with high-field susceptibility-weighted imaging. Medicine (Baltimore) 2023;102:e35003.
29. 29. Graff-Radford J, Arenaza-Urquijo EM, Knopman DS, et al. White matter hyperintensities: relationship to amyloid and tau burden. Brain 2019;142:2483–91.
30. 30. Lee S, Zimmerman ME, Narkhede A, et al. White matter hyperintensities and the mediating role of cerebral amyloid angiopathy in dominantly-inherited Alzheimer's disease. PLoS One 2018;13:e0195838.
31. 31. Holland CM, Smith EE, Csapo I, et al. Spatial distribution of white-matter hyperintensities in Alzheimer disease, cerebral amyloid angiopathy, and healthy aging. Stroke 2008;39:1127–33.
32. 32. Zamboni G, Griffanti L, Jenkinson M, et al. White Matter Imaging Correlates of Early Cognitive Impairment Detected by the Montreal Cognitive Assessment After Transient Ischemic Attack and Minor Stroke. Stroke 2017;48:1539–47.
33. 33. Greenberg SM, Eng JA, Ning M, et al. Hemorrhage burden predicts recurrent intracerebral hemorrhage after lobar hemorrhage. Stroke 2004;35:1415–20.
34. 34. Werring DJ, Gregoire SM, Cipolotti L. Cerebral microbleeds and vascular cognitive impairment. Journal of the Neurological Sciences 2010;299:131–5.
35. 35. Nakamori M, Hosomi N, Tachiyama K, et al. Lobar microbleeds are associated with cognitive impairment in patients with lacunar infarction. Sci Rep 2020;10:16410.
36. 36. Yu AC, Mohajer B, Eng J. External Validation of Deep Learning Algorithms for Radiologic Diagnosis: A Systematic Review. Radiol Artif Intell 2022;4:e210064.
37. 37. Gouw AA, Seewann A, Flier WM van der, et al. Heterogeneity of small vessel disease: a systematic review of MRI and histopathology correlations. Journal of Neurology, Neurosurgery & Psychiatry 2011;82:126–35.
38. 38. Yang Q, Wei X, Deng B, et al. Cerebral small vessel disease alters neurovascular unit regulation of microcirculation integrity involved in vascular cognitive impairment. Neurobiology of Disease 2022;170:105750.

Tables

Table 1: Baseline characteristics of participants

Variable	Training dataset (n = 287)	Internal validation dataset (n = 67)	External validation dataset (n = 68)	Clinical dataset (n = 448)	*P*
Age, years	68 ± 14	72 ± 10	53 ± 17	72 ± 9	< *.001*
Sex					.81
Male	116 (40.4)	27 (40.3)	32 (47)	171 (38.2)	
Female	171 (59.6)	40 (59.7)	36 (53)	277 (61.8)	
Diabetes	63 (22.0)	11 (16.4)	NA	119 (26.6)	.11
Hypertension	126 (43.9)	34 (50.7)	NA	219 (48.9)	.35
Hyperlipidemia	127 (44.3)	35 (52.2)	NA	180 (40.2)	.13
BMI (kg/m^2)*	24.2 ± 3.8	23.4 ± 3.4	NA	24.2 ± 3.3	.31
MMSE	24.7 ± 5.0	24.3 ± 4.8	NA	24.1 ± 5.3	.43
Total cholesterol (mg/dL)	173.2 ± 42.2	173.2 ± 56.9	NA	167.3 ± 38.3	.15
Triglycerides (mg/dL)†	121.0 ± 66.9	118.8 ± 64.6	NA	115.9 ± 65.8	.70
HDL (mg/dL)†	55.5 ± 14.3	56.0 ± 13.9	NA	55.2 ± 14	.91
LDL (mg/dL)†	97.2 ± 35.8	92.0 ± 38.4	NA	92.8 ± 32	.29
WMH burden (%)	3.9 ± 5.7	4.1 ± 5.4	NA	4.0 ± 5.1	.94
CMB present	154 (53.7)	67 (100)	22 (32.4)	287 (64.1)	
CMB number, median (IQR 25, 75)	1 (0, 3))	1 (1, 3))	0 (0, 1))	1 (0, 3))	.21

Note.—Mean data are ± SDs and numbers of participants with percentages in parentheses for categorical data.

BMI = body mass index, CMB = cerebral microbleed, HDL = high-density lipoprotein, LDL = low-density lipoprotein, MMSE = mini-mental status examination, WMH = white matter hyperintensity, NA = not applicable

*Number of participants with known BMI, n = 348

†Number of participants with known triglyceride, HDL, and LDL levels, n = 339

Table 2: Comparison of clinical variables between participants with cerebral microbleeds

Clinical variables	CMB present (n = 307)	CMB absent (n = 141)	*P*
Age	73 ± 9	69 ± 10	<.*001*
Sex			.08
Male	126 (41)	96 (68.1)	
Female	181 (59)	45 (31.9)	
Hypertension	158 (51.5)	61 (43.3)	.13
Diabetes	82 (26.7)	37 (26.2)	>.99
Hyperlipidemia	116 (37.8)	64 (45.4)	.16
BMI (kg/m^2)*	24.2 ± 3.6	24.2 ± 2.8	.98
MMSE	23.8 ± 5.5	24.8 ± 4.8	.053
Total Cholesterol (mg/dL)	165.3 ± 38.3	171.7 ± 38.2	.10
Triglyceride (mg/dL)†	115 ± 63.4	118.1 ± 71.4	.69
HDL (mg/dL)†	55.1 ± 13.5	55.7 ± 15.1	.71
LDL (mg/dL)†	91.9 ± 31.2	94.8 ± 33.6	.45
WMH burden (%)	4.8 ± 5.6	2.4 ± 3.2	<.*001*

Note.—Mean data are ± SDs and numbers of participants with percentages in parentheses for categorical data.

BMI = body mass index, CMB = cerebral microbleed, HDL = high-density lipoprotein, LDL = low-density lipoprotein, MMSE = mini-mental status examination, WMH = white matter hyperintensity

*CMB present (n = 237) and absent (n = 111)

†CMB present (n = 235) and absent (n = 104)

Table 3: Relationship between cognition (MMSE) and vascular risk factors

	Univariable linear regression			Multivariable linear regression		
Clinical variables	β	95% CI	*P*	β	95% CI	*P*
Age	-0.19	-0.24, -0.14	<.*001*	-0.14	-0.19, -0.09	<.*001*
Sex, male	0.87	-0.14, 1.88	.09	1.5	0.55, 2.45	.*002*
Hypertension	-0.33	-1.31, 0.66	.52			
Diabetes	-1.15	-2.26, -0.04	.*043*	-0.41	-1.5, 0.68	.47
Hyperlipidemia	1.51	0.52, 2.51	.*003*	1.88	0.96, 2.81	<.*001*
BMI (kg/m^2)	0.09	-0.07, 0.26	.27			
Total Cholesterol (mg/dL)	0.02	0.003, 0.03	.*014*	0.01	-0.003, 0.02	.14
Triglyceride (mg/dL)	0.004	-0.004, 0.01	.27			
HDL (mg/dL)	0.03	-0.01, 0.07	.15			
LDL (mg/dL)	-0.001	-0.02, 0.02	.87			
WMH burden (%)	-0.29	-0.38, -0.19	<.*001*	-0.17	-0.27, -0.08	<.*001*
Total CMB number	-0.014	-0.03, -0.006	.*006*	-0.01	-0.02, -0.001	.*04*

Note.— CI = confidence interval, BMI = body mass index, CMB = cerebral microbleed, HDL = high-density lipoprotein, LDL = low-density lipoprotein, MMSE = mini-mental status examination, SE = standard error, WMH = white matter hyperintensity

SUPPLEMENTAL FILES

Online Supplemental Data: Univariable linear regression between cerebral microbleed numbers and clinical variables

	Total			Lobar			Deep			Cerebellar		
Variables	β	95% CI	*P*	β	95% CI	*P*	β	95% CI	*P*	β	95% CI	*P*
Age	0.03	0.02, 0.04	<.001	0.02	0.02, 0.03	<.001	0.008	0.004, 0.013	*<.001*	0.007	0.002, 0.01	.007
Sex, male	0.17	-0.02, 0.36	.08	0.16	-0.02, 0.33	.07	0.009	-0.08, 0.09	.84	0.05	-0.05, 0.16	.29
Hypertension	0.33	0.14, 0.51	<.001	0.23	0.07, 0.4	.006	0.19	0.11, 0.27	*<.001*	0.14	0.04, 0.24	.005
Diabetes	0.16	-0.05, 0.37	.15	0.13	-0.06, 0.32	.18	0.06	-0.03, 0.15	.21	0.08	-0.03, 0.19	.16
Hyperlipidemia	0.03	-0.16, 0.22	0.77	0.01	-0.16, 0.18	.89	0.04	-0.04, 0.13	.33	0.07	-0.03, 0.17	.19
BMI (kg/m^2)	-0.02	-0.06, 0.008	.14	-0.03	-0.06, 0.001	.06	0.001	-0.01, 0.01	.88	-0.007	-0.02, 0.01	.42
WMH burden (%)	0.08	0.06, 0.1	*<.001*	0.07	0.05, 0.09	*<.001*	0.04	0.03, 0.05	*<.001*	0.02	0.01, 0.03	*<.001*
Total Cholesterol (mg/dL)	-0.003	-0.006, -0.001	.007	-0.003	-0.005, -0.001	.005	-0.002	-0.003, -0.001	*.002*	-0.0008	-0.002, 0.001	.25
Triglyceride (mg/dL)	0.0003	-0.001, 0.002	.68	0.0002	-0.001, 0.002	.82	0.00003	-0.0003, 0.001	.34	0.0001	-0.0007, 0.001	.75
HDL (mg/dL)	-0.003	-0.01, 0.004	.36	-0.002	-0.009, 0.005	.61	-0.003	-0.007, -0.0002	.04	-0.003	-0.007, 0.001	.11
LDL (mg/dL)	-0.003	-0.006, 0.0001	.06	-0.003	-0.006, -0.0005	.02	-0.001	-0.003, 0.001	.07	-0.0005	-0.002, 0.001	.54

Note.— CI = confidence interval, BMI = body mass index, HDL = high-density lipoprotein, LDL = low-density lipoprotein, SE = standard error, WMH = white matter hyperintensity. Total, lobar, deep, and cerebellar cerebral microbleeds were log-transformed.

Table S1. Checklist for Artificial Intelligence in Medical Imaging (CLAIM): 2024 Update

Section / Topic	No.	Item	Page / Line	No	NA
TITLE / ABSTRACT					
	1	Identification as a study of AI methodology, specifying the category of technology used (e.g., deep learning)	**1**		
ABSTRACT					
	2	Summary of study design, methods, results, and conclusions	**1**		
INTRODUCTION					
	3	Scientific and/or clinical background, including the intended use and role of the AI approach	**2/25**		
	4	Study aims, objectives, and hypotheses	**2/34**		
METHODS					
Study Design	**5**	Prospective or retrospective study	**2/41**		
	6	Study goal	**2/34**		
Data	**7**	Data sources	**2/45**		
	8	Inclusion and exclusion criteria	**2/49**		

	9	Data pre-processing	**3/68**		
	10	Selection of data subsets			**V**
	11	De-identification methods	**2/41**		
	12	How missing data were handled			**V**
	13	Image acquisition protocol	**2/61**		
Reference Standard	**14**	Definition of method(s) used to obtain reference standard	**3/71**		
	15	Rationale for choosing the reference standard			**V**
	16	Source of reference standard annotations			**V**
	17	Annotation of test set	**2/68**		
	18	Measures of inter- and intra-rater variability of features described by the annotators			**V**
Data Partitions	**19**	How data were assigned to partitions	**2/46**		
	20	Level at which partitions are disjoint	**2/45**		
Testing Data	**21**	Intended sample size		**V**	
Model	**22**	Detailed description of model	**3/80**		
	23	Software libraries, frameworks, and packages	**3/81**		
	24	Initialization of model parameters			**V**
Training	**25**	Details of training approach	**3/80**		
	26	Method of selecting the final model	**3/85**		
	27	Ensembling techniques			**V**
Evaluation	**28**	Metrics of model performance	**3/85**		
	29	Statistical measures of significance and uncertainty	**3/115**		
	30	Robustness or sensitivity analysis	**3/84**		
	31	Methods for explainability or interpretability	**3/85**		
	32	Evaluation on internal data	**Table 1**		
	33	Testing on external data	**2/56**		
	34	Clinical trial registration			**V**
RESULTS					
Data	**35**	Numbers of patients or examinations included and excluded	**5/127**		
	36	Demographic and clinical characteristics of cases in each partition	**Table 1**		
Model performance	**37**	Performance metrics and measures of statistical uncertainty	**5/139**		
	38	Estimates of diagnostic performance and their precision	**5/139**		
	39	Failure analysis of incorrect results			**V**
DISCUSSION					
	40	Study limitations	**9/255**		
	41	Implications for practice, including intended use and/or clinical role	**10/273**		
OTHER INFORMATION					
	42	Provide a reference to the full study protocol or to additional technical details	**3/91**		
	43	Statement about the availability of software, trained model,	**3/91**		

		and/or data			
	44	Sources of funding and other support; role of funders			**V**

Table S2: MRI acquisition parameters

Parameter	T2 FLAIR	T2WI	SWI	3D T1WI
Repetition time (msec)	9000	3000	31	6.3
Echo time (msec)	125	80	7.2	2.9
Echo time spacing (msec)	NA	NA	6.2	NA
Inversion time (msec)	2500	NA	NA	NA
Flip angle (degree)	90	90	17	9
No. of averages	1	1	1	1
Matrix	256×256	384×384	368×297	256×256
Section thickness (mm)	3	4	2	1
Intersection gap (mm)	0	0	0	0
Field of view (mm2)	220×220	220×220	220×178	256×256
Total scan time	3 min 36 sec	2 min 33 sec	3 min 3 sec	6 min 11 sec

Note.—3D = three-dimensional, FLAIR = fluid-attenuated inversion recovery, NA = not applicable, SWI = susceptibility weighted image, T1WI = T1-weighted image, T2WI = T2-weighted image

Table S3: MRI Characteristics of External Datasets

Sites	Sex	Age	MR manufacturer	MR model	In-plane resolution (mm^2)	Slice thickness (mm)	Ground Truth CMB count	Predicted CMB count	TN/FN/FP/TP†	DSC‡
1	F	32	Philips	Achieva	0.47 × 0.47	3	0	0	TN	
	M	49	Philips	Ingenia	0.47 × 0.47	3	0	0	TN	
2	F	55	Philips	Ingenia Elition X	0.34 × 0.34	1	0	0	TN	
3	M	55	Siemens	VIDA	0.53 × 0.53	2	0	0	TN	
	M	43	Siemens	VIDA	0.53 × 0.53	2	0	0	TN	
4	F	19	Siemens	Essenza*	0.72 × 0.72	1.6	0	0	TN	
5	F	78	Siemens	Skyra	0.45 × 0.45	2	0	0	TN	
	F	76	Philips	Ingenia CX	0.33 × 0.33	1	0	1	FP	
6	F	29	Philips	Ingenia Elition X	0.43 × 0.43	1.5	0	0	TN	
7	F	73	Siemens	Skyra	0.25 × 0.25	2.5	0	0	TN	
8	F	68	GE	Signa Pioneer	0.47 × 0.47	1	1	1	TP	0.02
9	M	20	GE	Premier	0.45 × 0.45	2	0	0	TN	
10	M	74	Siemens	Verio	0.57 × 0.57	1.5	1	1	TP	0.4
11	M	54	Siemens	Skyra	0.75 × 0.75	1	0	0	TN	
	M	61	Philips	Ingenia	0.5 × 0.5	3	0	0	TN	
12	M	63	Siemens	VIDA	0.55 × 0.55	2	170	88	FN	0.36
13	F	48	Philips	Ingenia	0.43 × 0.43	2	0	0	TN	
	M	38	Philips	Ingenia	0.43 × 0.43	2	3	3	TP	0.7

										3
14	F	50	Philips	Ingenia Elition X	0.31 × 0.31	1	0	0	TN	
15	F	31	Siemens	VIDA	0.45 × 0.45	4	0	0	TN	
16	M	80	Philips	Ingenia CX	0.29 × 0.29	1	7	7	TP	0.7
	M	66	Philips	Ingenia CX	0.29 × 0.29	1	1	1	TP	0.78
	M	29	Siemens	Symphony Tim*	0.75 × 0.75	1.6	4	0	FN	0
	F	54	Philips	Ingenia CX	0.29 × 0.29	1	0	0	TN	
17	F	25	Siemens	VIDA	0.36 × 0.36	2	0	0	TN	
	M	76	Siemens	Skyra	0.49 × 0.49	3	0	0	TN	
	M	55	Siemens	Skyra	0.49 × 0.49	3	0	0	TN	
18	F	35	Siemens	VIDA	0.55 × 0.55	2	0	0	TN	
19	F	49	Siemens	Verio	0.49 × 0.49	2	0	0	TN	
	M	61	Siemens	Verio	0.47 × 0.47	2	0	1	FP	
	F	30	Siemens	Verio	0.45 × 0.45	2	0	1	FP	
20	M	38	GE	Signa Architect	0.43 × 0.43	1.5	0	1	FP	
	F	46	Philips	Ingenia Elition X	0.31 × 0.31	1	0	0	TN	
21	F	59	Philips	Achieva	0.41 × 0.41	0.8	2	2	TP	0.72
22	M	54	Siemens	Sempra*	0.9 × 0.9	2	0	1	FP	
23	M	68	Siemens	VIDA	0.57 × 0.57	1	17	9	FN	0.45
	F	47	Siemens	Skyra	0.49 × 0.49	1	0	0	TN	
24	F	33	Philips	Ingenia Elition X	0.43 × 0.43	1	0	0	TN	
25	F	56	Philips	Ingenia CX	0.43 × 0.43	2	1	1	TP	0.75
26	M	71	Siemens	Verio	0.72 × 0.72	2	2	0	FN	0
27	M	75	Siemens	Verio	0.36 × 0.36	1	0	1	FP	
28	M	22	Philips	Achieva	0.25 × 0.25	5	0	0	TN	
	F	82	Philips	Ingenia	0.25 × 0.25	5	5	5	TP	0.76
29	M	65	Siemens	VIDA	0.6 × 0.6	2	1	1	TP	0.76
30	F	58	GE	Signa Architect	0.43 × 0.43	1.2	0	0	TN	
31	M	59	Philips	Achieva	0.24 × 0.24	1.5	0	0	TN	
32	M	61	Siemens	Skyra	0.72 × 0.72	2	0	1	FP	
	F	40	Siemens	Skyra	0.72 × 0.72	2	1	0	FN	0
33	F	31	Siemens	Magnetom Lumina	0.43 × 0.43	2	0	0	TN	
34	M	59	Philips	Achieva	0.45 × 0.45	1.5	2	2	TP	0.7
35	F	44	Siemens	Magnetom Lumina	0.45 × 0.45	1.5	0	0	TN	
36	M	50	Philips	Ingenia CX	0.45 × 0.45	1	4	4	TP	0.77

37	M	66	Philips	Achieva dStream	0.45 × 0.45	0.85	0	0	TN	
38	M	57	Siemens	Skyra	0.69 × 0.69	1.5	0	0	TN	
39	M	78	Philips	Achieva dStream	0.37 × 0.37	1.5	1	1	TP	0.76
40	F	61	Philips	Ingenia CX	0.41 × 0.41	1.5	0	0	TN	
	F	66	Philips	Ingenia	0.43 × 0.43	1.5	1	3	FP	0
41	M	74	Philips	Ingenia CX	0.3 × 0.3	1	1	3	FP	0.12
	F	34	Philips	Ingenia CX	0.3 × 0.3	1	2	1	FN	0.56
	F	56	Philips	Ingenia CX	0.3 × 0.3	1	1	1	TP	0.63
42	F	60	Siemens	Avanto*	0.75 × 0.75	2.5	0	0	TN	
43	F	62	Philips	Ingenia	0.3 × 0.3	1	4	4	TP	0.13
44	M	21	Siemens	VIDA	0.57 × 0.57	2	0	0	TN	
45	F	31	Philips	Ingenia CX	0.42 × 0.42	1	0	0	TN	
46	F	35	Siemens	Sempra*	0.4 × 0.4	2	0	2	FP	
47	M	65	Siemens	Verio	0.57 × 0.57	2	0	0	TN	
48	F	81	Siemens	VIDA	0.31 × 0.31	1	0	0	TN	
49	F	31	Philips	Ingenia CX	0.29 × 0.29	1	0	1	FP	

Note.—CMB = cerebral microbleed, DSC = dice similarity coefficient, FN = false negative, FP = false positive, TN = true negative, TP = true positive

*1.5-Tesla

†Accuracy = 75.0% (63.6–83.8%), Sensitivity = 70.0% (48.1–85.5%), Specificity = 77.1% (63.5–86.7%)

‡Calculated for cases with ground truth CMB masks

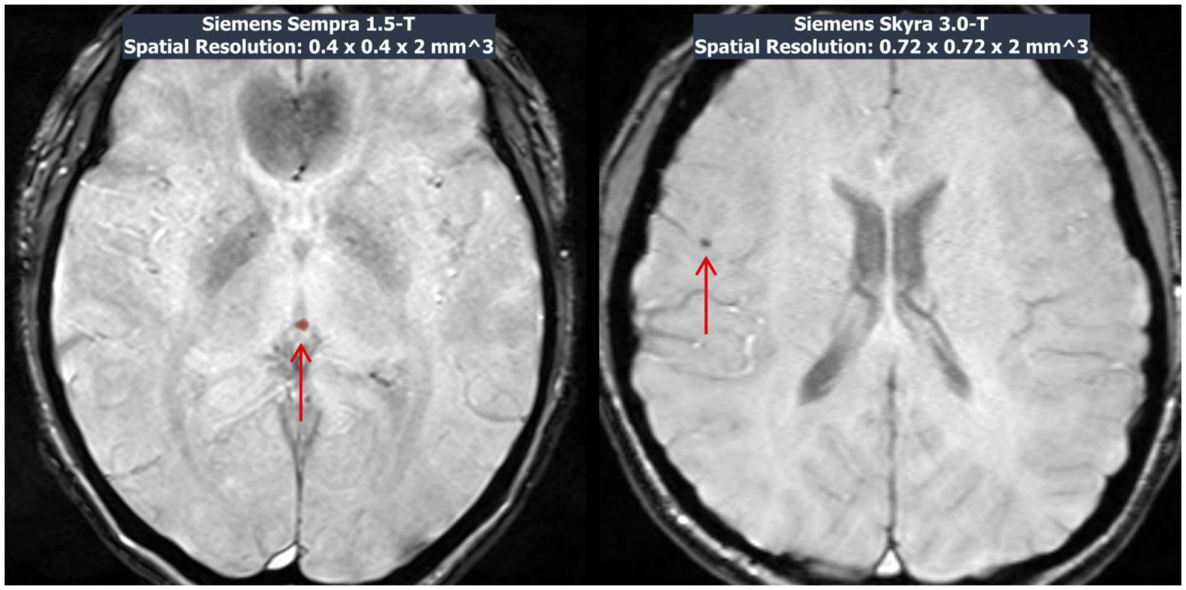

Figure S1. Example images of false positive segmentation of pineal gland calcification (left) and false negative detection of CMB (right) in the external validation dataset. The MR scanner model names and spatial resolutions are displayed at the top.

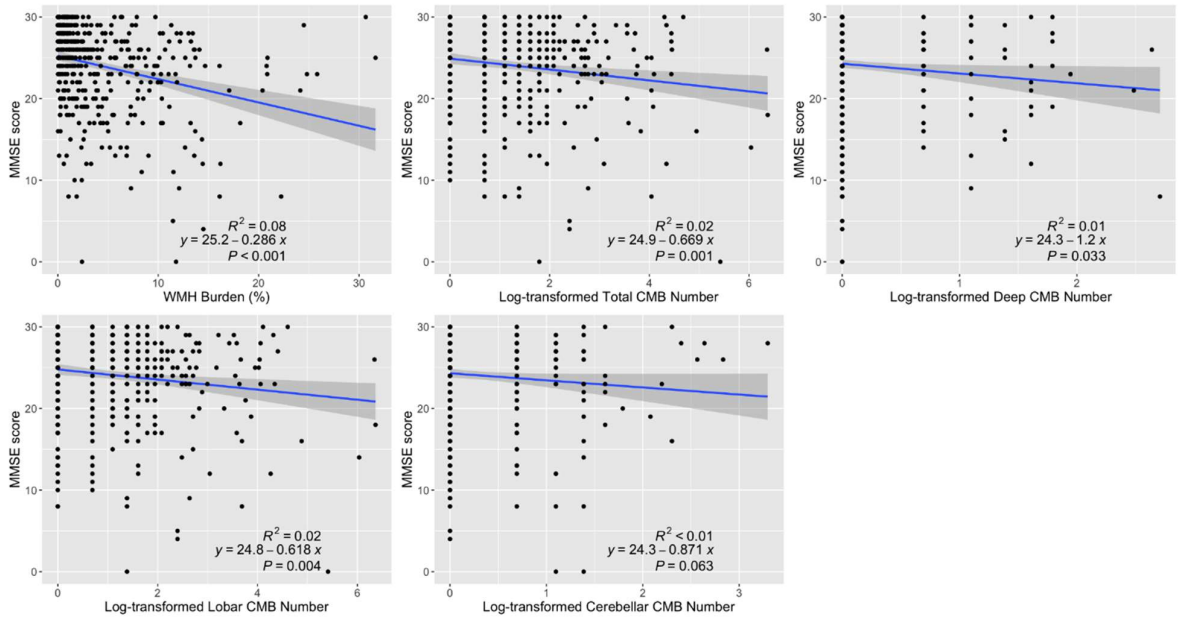

Figure S2. Relationship between MMSE scores and log-transformed CMB number/WMH burden. Solid blue lines indicate the lines of best fit for linear regression, while the shaded areas indicate the 95% confidence intervals. The R^2 values are the linear regression coefficients of determination.